Rheol. Acta 15, 242–255 (1976)

Laboratory of Physical Chemistry, Delft University of Technology, Delft (The Netherlands)

A re-designed cone-and-plate apparatus for the measurement of the flow birefringence of polymer melts*)

*F. H. Gortemaker, M. G. Hansen**), B. de Cindio***), and H. Janeschitz-Kriegl*

With 15 figures and 1 table

(Received March 18, 1976)

1. Introduction

Flow birefringence may be considered as one of the more productive experimental methods suitable for the investigation of the rheological properties of polymeric systems. The main advantage of this method lies in the possibility to obtain a rather accurate knowledge of the state of stress in a flowing polymer, without using a mechanical measuring device.

The operational principles of flow birefringence were extensively described by one of the present authors in his review article (1). We are interested in the relationship between the optical and mechanical properties of the melt. These properties may be described in terms of the refractive index and the stress ellipsoids. The link between these two tensors is formed by the so-called "stress-optical law", which claims the proportionality between the deviatoric tensor components (i.e. $\Delta n = C \cdot \Delta p$). It also includes the coaxiality of the mentioned ellipsoids.

As far as solutions were concerned, the validity of the stress-optical law has been substantiated for steady shear flow over wide ranges of shear rates and concentrations, and for various types of polymers by a number of authors (1–6). The validity of the stress-optical law, however, has been questioned for transient flow by *Janeschitz-Kriegl* (1), *Wayland* (7) and *Harris* (8) but no experimental results were presented. The first attempt to check the stress-optical law experimentally for the transient region in slow shear flow of a polymer melt was made by *Janeschitz-Kriegl* and *Gortemaker* (9). Additionally, only few experimental results are available for steady shear flow of polymer melts at high shear rates (10, 11).

In this paper, a cone-and-plate apparatus will be described. This apparatus was originally designed to furnish information on steady shear flow, in a range of shear rates higher than usually accessible in a cone-and-plate apparatus. At the same time, however, this apparatus happened to give reasonably accurate results also in the low shear rate range for fluids responding rather slowly to a step in the shear rate.

Some typical flow birefringence measurements will be presented for three commercial polymer melts over a wide range of shear rates. In order to check the stress-optical law, use is made of additional oscillatoric mechanical and capillary viscometer measurements.

Also some typical measurements in the transient region of slow flow are presented to show the rather wide applicability of the apparatus. In this connection some results of measurements on a Weissenberg rheogoniometer, as kindly supplied by Drs. *Laun* and *Münstedt* (BASF Ludwigshafen), are also incorporated.

Numerical analysis of the flow was performed to obtain an understanding of the actual velocity profiles for different nominal shear rates. In this way also an estimate could be made of the influence of frictional heat on the experimental results.

2. Description of the apparatus

The experimental set-up consists of three different main parts, which will be described separately: the cone-and-plate apparatus containing the test section, the optical system and the driving system.

*) The present investigation has been carried out under the auspices of the Netherlands Organization for the Advancement of Pure Research (Z. W. O.).

**) North Atlantic Treaty Organization Science Post Doctoral Fellow.

***) On leave from University of Naples; Research Fellow, Delft University of Technology.

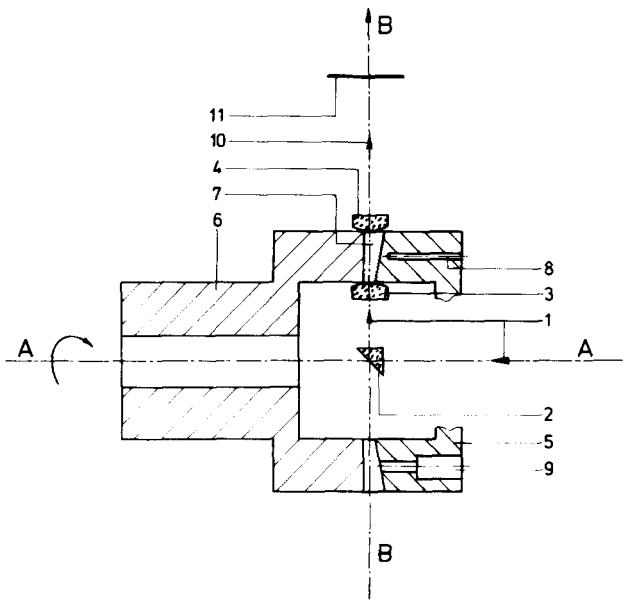

Fig. 1. Cross-section through heart of cone-and-plate system. (1) linearly polarized light beam, (2) reflection prism, (3) inner window, (4) outer window, (5) stationary cone, (6) rotating plate, (7) test section, (8) blind hole for the thermocouple, (9) sample injection hole, (10) elliptically polarized light beam, (11) analyser

The operational principle of the cone-and-plate apparatus is illustrated in fig. 1. As already pointed out, the apparatus is similar to the one described by *Wales* and *Janeschitz-Kriegl* (12). In both designs there are no free surfaces of the sample. The test section pos. 7 is an annulus bounded by the rotating plate pos. 6, the stationary cone pos. 5 and the stationary inner and outer cylindrical surfaces. These surfaces are formed by an inner cylindrical part located in the centre of the ring and by an outer cylindrical part on which the heating elements are arranged. It appears that the complete enclosure of the sample achieved in this way effectively reduces degradation, which evidently occurs, if the rim of the sample is in contact with air. The test section is filled by injecting molten polymer through a hole pos. 9 made in the stationary cone. As the polymer is forced into the apparatus, the air contained in the gap can apparently escape through the narrow clearances between the parts. Two glass windows (optical glass BK 7, Schott and Gen. (Borfe)) pos. 3 and pos. 4 are located along a major diameter (B – B) in the cylindrical bounding surfaces of the test section. This type of glass has a low thermal cubic expansion coefficient ($2.3 \times 10^{-5}\,°C^{-1}$) and a low residuel birefringence.

This apparatus represents a further development of the previously mentioned one (12) being essentially different only with respect to the propagation of light. In fact, with respect to the earlier apparatus, the direction of the light beam is reversed, following a suggestion of *Wales*. The explanation for this change will be given below. In the present arrangement, the light enters from the right along the axis A – A, and is reflected by means of a glass prism pos. 2 which is located in the centre of the inner cylindrical part. This prism reflects the light radially outwards along the line B – B.

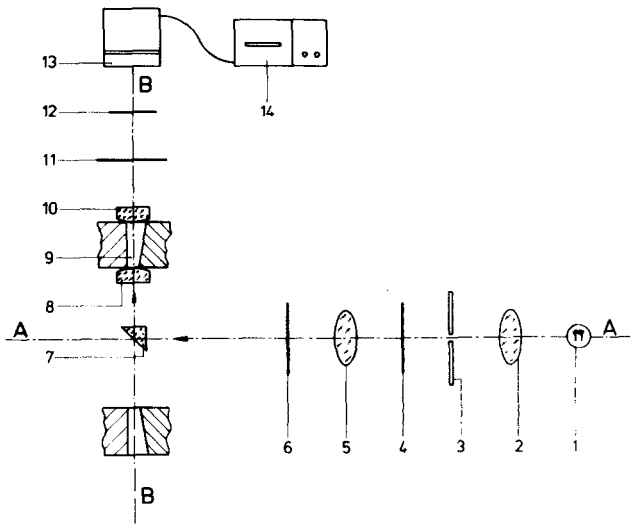

Fig. 2. Schematic drawing of the optical measurement system: (1) high pressure mercury lamp, (2) lens, (3) aperture, (4) interference filter, green 546 nm, (5) lens, (6) polarizer, (7) reflection prism, (8) inner window, (9) polymer sample, (10) outer window, (11) Ehringhaus compensator, (12) analyser, (13) photomultiplier, (14) high speed (ultra-violet light beam) recorder

A scheme of the optical system is presented in fig. 2. The light source pos. 1 is a high pressure mercury lamp. Optical elements along the line A – A are positioned to focus the light beam through the test section. Linearly polarized light is obtained by means of a polarizing sheet (POLAROID HN 22 × 0.35") pos. 6. An analyser pos. 12 of the same type as the polarizer is located after the upper window. Between the upper window and the analyser, there is a holder pos. 11 for a compensator which enables the measurement of the birefringence. A filter pos. 4 (Interference filter Filtraflex-B-10, manufactured by Balzers with a wavelength of 546.1 nm and a tolerance of $\pm 0.15\%$) is inserted into the beam to produce monochromatic light.

The system built in this way is a typical linear polariscope (13) with crossed polarizer and analyser (dark field). The optical elements from pos. 1 to 6 of the figure are mounted on an optical bench which hinges on the line B – B. Also the prism, the two windows and the analyser are rotated around the same line B – B, being rigidly connected to the hinged optical bench. Hence, the vertically (or horizontally) polarized incident beam always remains polarized parallel (or perpendicular) to the incidence plane of the reflection prism. Therefore, the state of linear polarization of the incident beam remains uneffected by the prism[1]). A vernier scale permits the reading of the angle of rotation of the optical bench around B – B. In this way the determination of the position of the polarization direction with respect to the flow field is achieved.

When the sample is deformed by the flow, it becomes optically anisotropic and shows extinction positions and a certain amount of birefringence. Usually, the extinction angle χ is defined as the angle smaller than forty-five degrees, occurring between one of the extinction positions and the direction of the streamlines. To determine χ, the direction of polarization is rotated until it is aligned with the corresponding axis of the refractive index ellipsoid. This is achieved by rotating the optical bench around the line B – B until the intensity of the light beam emerging from the analyser is minimized. Then a reading is made from the vernier scale. The indeterminateness of the zero-position of the vernier scale is eliminated by making another reading for the reversed flow direction. Half of the difference between these readings gives the extinction angle χ. The zero-position is obtained by averaging these values. The birefringence Δn is measured after the insertion of the Ehringhaus compensator (manufactured by Carl Zeiss) in the previously mentioned holder and insertion of monochromatic filter at pos. 4, fig. 2. The principle of operation of this type of compensator is described in the literature (14).

The scheme of the driving system is depicted in fig. 3. It consists of a synchronous motor, which is fed by a frequency synthesizer in order

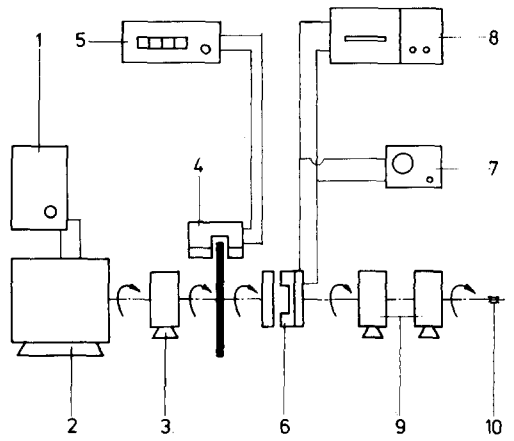

Fig. 3. Schematic of cone-and-plate apparatus, drive system: (1) frequency synthesizer, (2) synchronous motor, (3) gearbox, (4) chopped light tachometer, (5) electronic counter, (6) electrical magnetic cluth, (7) clutch control clock, (8) high speed (ultra violet light beam) recorder, (9) gearboxes, (10) rotating plate coupling

to supply a stepless speed control over one decade of frequency. A wide range of shear rates is obtained with the aid of an assemblage of interchangeable speed reduction gear-boxes. The rotational speed is measured by a chopped-light tachometer connected to an electronic counter. The constancy of the drive is within 0.1%. The rotating plate of the test section is connected (through one of the gear-boxes) to the driving system by means of an electrical magnetic clutch. The engagement and disengagement of the clutch is controlled by a clock. The response of the clutch has been determined with the empty test section. It was measured that full speed of the rotor is achieved within 10 ms.

This drive system enables the investigation of material transient response to a step- and boxlike function of shear rate. Thus, stress growth after a period of rest, stress relaxation after a certain amount of shear and stress relaxation after steady shear flow can be investigated. For these types of measurements the signal from the clutch can be recorded on an ultra-violet light recorder as shown in fig. 3.

At this point it should be admitted that the development of high speed recording is not yet finished. The change of extinction angle with time is readily measured by recording the times at which the isocline passes several presettings of the crossed polarizers with the photomultiplier tube pos. 13 and ultra-violet light recorder pos. 14 of fig. 2. However, the handling of the

[1]) In the original version (12), corrections were necessary for the change which the elliptically polarized light emerging from the test section, undergoes in the reflection prism.

Ehringhaus compensator is much too time consuming for rapidly responding materials. In order to improve recording speed and accuracy the following two modifications were made:

i) modulation of the birefringence with the aid of a rotating mica plate, in order to measure weak but quickly changing birefringences,
ii) the utilization of circularly polarized light in order to avoid interference of isoclines and fringes and thus to enable undisturbed counting of quickly passing fringes, when the birefringence becomes large.

Finally, we shall make some comments on the temperature control. Several heating elements are positioned around the test section. A check for the absence of any temperature gradient in the gap was made in the empty test section. Two thermocouples were used (see fig. 1): one was inserted into the test section through the injection hole (pos. 9), while the other one was located at the bottom of a blind hole (pos. 8) in the stationary cone, near the windows. The distance from the cone surface to the bottom of the hole is 1 mm. In this way we were able to measure the temperature in two diametrically opposite points of the gap. The temperature difference between these two points was less than 0.2 °C. This confirms that no appreciable temperature gradients are present in the gap due to the non-uniform distribution of the heating elements. The temperature during the test is measured by means of a thermocouple inserted in the blind hole.

3. Materials and rheological characterization

Three different commercial polymers have been used: a high density polyethylene (Manolene 6050), a low density polyethylene (sample A (22–24)) and a polystyrene (Hoechst).

The samples were made starting from pellets, which were put into a cylindrical heated mould and melted under vacuum. Then the material was compressed and cooled under pressure. The value of the pressure was about 1.5×10^7 $N \cdot m^{-2}$. In this way a cylindrical bar (with a diameter of 2 cm and a length of 15 cm) is obtained. This bar is mechanically machined to obtain the right shape and size of the injected sample.

In order to check the kinematics of our system and the validity of the stress-optical law, a rheological characterization of the polymers was necessary. For this purpose, the steady shear flow curves over a rather wide range of shear rates were measured. This was achieved with the aid of different mechanical tests. Capillary viscometry was applied to obtain the flow curves in the high shear rate region. Dynamic mechanical measurements were used to enable extrapolation of viscosity-shear rate curves to low shear rates, where capillary viscometry fails.

Values of steady state viscosity at different shear rates were determined using a capillary viscometer designed by *J. van Leeuwen* and *R. van der Vijgh* at the Plastic and Rubber Institute T.N.O. (Delft). The data were corrected according to *Bagley* (15) for entrance effects. The shear rate q was evaluated at the wall according to *Rabinowitsch* (16). The covered range of shear rates is from $1\ s^{-1}$ to about $1000\ s^{-1}$.

Values of the storage and loss moduli (G' and G'') at rather low circular frequencies ω, were obtained with the aid of an automatic dynamic viscometer, designed by *K. te Nijenhuis* at this laboratory. This apparatus is an improved version of *Den Otters'* dynamic viscometer (17, 18). It allows the obtaining of accurate data also in the range of very low frequencies where the phase angle differs only little from ninety degrees. Details of this apparatus will be published in due course. The values of G' and G'' were obtained as functions of frequency and temperature. Use was made of the time-temperature superposition principle (19) in order to obtain master curves over an extended range of frequencies at the chosen reference temperature (179 °C for the high density polyethylene).

An empirical relation, proposed by *Cox* and *Merz* (20), was used to obtain the steady shear viscosity η as function of the shear rate q from the reduced values of G' and G''. This relation reads:

$$\eta(q) = |\eta^*(\omega)|_{\omega = q} \qquad [1]$$

where $|\eta^*(\omega)|$ is the absolute value of the complex viscosity defined as follows:

$$\eta^*(\omega) = \eta'(\omega) - i \cdot \eta''(\omega) \qquad [2]$$

with

$$\eta'(\omega) = G''(\omega)/\omega\,, \qquad [3]$$

$$\eta''(\omega) = G'(\omega)/\omega\,. \qquad [4]$$

At low shear rates or frequencies relations [1] and [3] converge to the correct value of the zero shear viscosity.

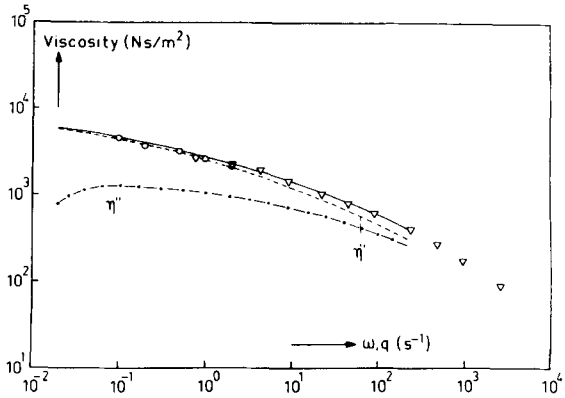

Fig. 4. Non-Newtonian shear viscosity $\eta(q)$ as a function of shear rate q as obtained with the following instruments: (▽)... capillary viscometer, (○)... cone-and-plate viscometer (plate diameter 50 mm, gap angle 8 degrees). For comparison, the figure contains the absolute value of the complex viscosity (full line), the real part of the dynamic viscosity η' (–––––) and the imaginary part of the dynamic viscosity η'' (–·–·–) as functions of the circular frequency ω. (High density polyethylene Manolene 6050, at a temperature of 179°C)

The resulting curve is shown in fig. 4. A good agreement between the capillary shear viscosity and the value computed from dynamic data is found in the central range of shear rates where the curves overlap. The agreement is still rather good in the high shear rate range. Some additional steady shear viscosity data are included in the region of low shear rates. These data were obtained with the aid of a cone-and-plate Weissenberg rheogoniometer. Within the experimental error, these data also agree with the values computed from the dynamic measurements.

The rheological properties of the low density polyethylene are already extensively described by *Wales*, *Meissner* and *Hansen* (22–24).

4. Kinematics

The geometry of the test section has been described in section 2. Usually cone-and-plate viscometers have a free boundary at the edge. In birefringence measurements this surface would disturb the light propagation. This is one of the reasons why in our system the test section is completely enclosed by fixed cylindrical surfaces containing the windows. In this connection some considerations have to be made in order to ensure that the flow field is essentially that of a homogeneous shear flow. The problems which arise in this geometry are well-known from any type of rheometer in which the shear rate is undefined at the geometric intersection of two surfaces, one of them moving with respect to the other. In such an apparatus an approximately homogeneous shear flow can be obtained at best. Depending on the geometry, the polymer used and the temperature given, this approximation is tolerable only in a certain range of shear rates. Therefore it is crucial to estimate the velocity profiles for every tested polymer.

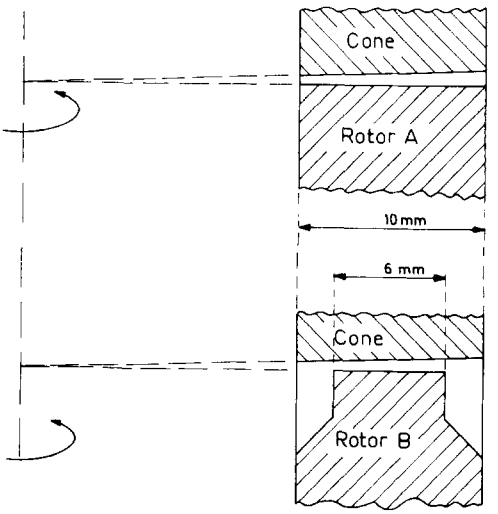

Fig. 5. Principles of the different rotors

Two different rotors have been used. Schematic drawings of them are shown in fig. 5. Also two cones (counter parts) of different gap angle (1° 8′ and 2° 17′) were available.

Using rotor A, one obtains a cone-and-plate arrangement enclosed in the radial direction between fixed cylindrical surfaces. In this way, the rotating surface intersects close to the windows, with the stationary boundary, producing just in this zone a very inhomogeneous shear flow.

From experience we know that this geometry is only suitable for relatively low nominal shear rates (21). In fact, *Wales* explains the failure of this geometry at high nominal shear rates in terms of the rather strong birefringence which is due to this inhomogeneous zone of flow near the windows. As is well-known, the passage through several zones of strong, but differently oriented birefringences causes serious depolarization of

polarized light. A second rotor B has been designed to move the line of singularity away from the optical path. It was expected that in this way measurements would be possible at higher nominal shear rates. It will be clear that in this new rotor system the effective optical path length is less than 10 mm but more than 6 mm. To calculate that effective path length an approximative numerical computation (25) of the velocity and temperature profiles was made for rotor *B*. The change of the viscosity with shear rate and temperature was taken into account by the use of a relation combining the inelastic "power law" concept with an experimental temperature coefficient. This model is sometimes called the generalized Newtonian model as elastic effects are disregarded. One obtains:

$$\eta = 2^{-2\alpha}\eta_1 I_2^{-\alpha} e^{-b(T-T_R)}. \qquad [5]$$

In this equation α describes the shear rate dependence and b the temperature dependence of the viscosity, η_1 is a constant, I_2 is the second invariant of the rate of strain tensor and T_R the reference temperature. For the investigated high density polyethylene constants η_1 and α can be calculated from fig. 4, if for the range of interesting shear rates the real curve is approximately replaced by a straight line. The constant b was calculated from the horizontal shift factor a_T of the dynamic measurements.

The required constants for Manolene 6050 as obtained for $10 < q < 1000\,s^{-1}$, are given in tab. 1.

To make computations easier the actual flow was replaced by the flow in a straight channel.

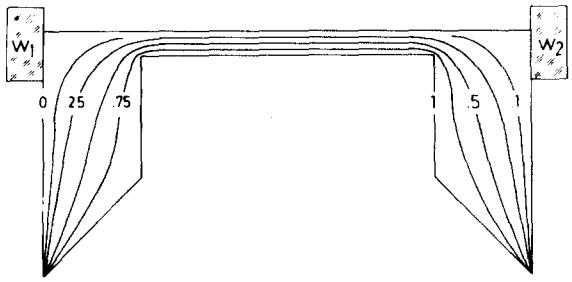

Fig. 6. Dimensionsless velocity field for rotor B, computed with the aid of eq. [5] for high density polyethylene Manolene 6050 at a temperature of 179 °C and a nominal shear rate $q_n = 100\,s^{-1}$. W1, W2 are the inner and outer window of the test section

Tab. 1. Constants in eq. [5] for Manolene 6050

η_1 =	4940	($N \cdot sec^{1-2\alpha}/m^2$)
α =	0.23	(– –)
b =	0.188	($°C^{-1}$)
T_R =	179	(°C)

The surface of the cone was replaced by a flat surface parallel to the top of the ridge which replaces rotor *B*.

The dimensionless velocity field for the approximated rotor B geometry is presented in fig. 6 for Manolene 6050 at 179 °C and a shear rate $q_n = 1000\,s^{-1}$. It is clear from this graph that the lines of singularity are moved away from the optical path. From this type of velocity profiles it is possible to compute the actual velocity gradients in the gap. The results are collected for several fluid models in fig. 7. In this figure x is the direction of flow, y the direction of the "main" velocity gradient and z the direction of the light-beam. The values of

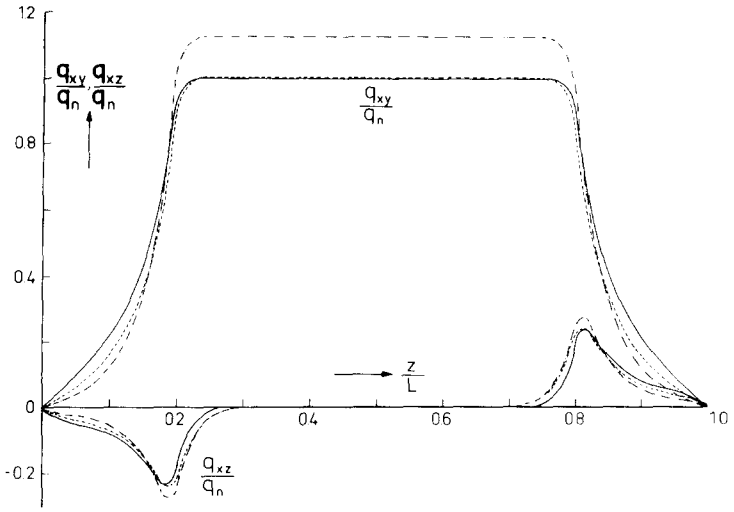

Fig. 7. Dimensionless velocity gradients q_{xy}/q_n and q_{xz}/q_n in the central plane of the test section of rotor B as functions of the reduced distance from one of the windows: computation for an isothermal Newtonian fluid ... (———); computations with the aid of eq. [5] for high density polyethylene Manolene 6050 at a wall temperature of 179 °C and nominal shear rates: $q_n = 100\,s^{-1}$ ... (– – –) and $q_n = 1000\,s^{-1}$ ... (– · – · –)

the "main" velocity gradient $\partial V_x/\partial y = q_{xy}$ and the "parasitic" velocity gradient $\partial V_x/\partial z = q_{xz}$ are divided by the nominal shear rate q_n to obtain a dimensionless quantity. The nominal shear rate is equal to the one, which would occur with free boundaries at the edges (viscometric shear flow). The dimensionless velocity gradients are taken in the central $x-z$ plane of the test section and are plotted as functions of the reduced distance from one of the windows. It appears from this figure that there is, at $q_n = 100\,s^{-1}$ only a very small difference between the results for an isothermal Newtonian fluid and the model applied for Manolene 6050. For nominal shear rates increasing beyond $100\,s^{-1}$, however, the actual velocity gradient q_{xy} starts to become considerably larger than the nominal shear rate. This effect is due to the occurrence of noticeable temperature gradients in the melt, as a consequence of viscous dissipation. The "parasitic" velocity gradient q_{xz} seems to be small compared with q_{yz} in all cases.

Further, it is important to know the length of the effective light path, which has to be used for evaluation of the birefringence measurements. For this purpose, an estimate has to be made of the influence of the zone in which q_{xy} is less than the nominal shear rate. As long as a fluid shows Newtonian behaviour, for viscometric shear flow the extinction angle χ is equal to 45° and the birefringence Δn is proportional to the shear rate. This means that any "parasitic" birefringence as caused by the "parasitic" gradient q_{xz} does not influence the measurement of the "main" birefringence. As a matter of fact, due to the direction of the "parasitic" velocity gradient, the extinction position of any parasitic birefringence must be parallel and perpendicular to the direction of the stream lines. In other words, its extinction is under 45° with that of the "main" birefringence. This means that the parasitic birefringence is not "seen" during the measurement of the main optical path difference (see e.g. Appendix). For such a case one can unambiguously calculate an effective length of the gap by integrating the curve giving q_{xy}/q_n as a function of z/L, from zero to unity (see fig. 7) and multiplying the result by L. For the Newtonian case this procedure is correct, since the local increment $\Delta n\,dz$ to the phase difference is simply proportional to $q_{xy}\,dz$. In this way one obtains an effective path length of 7.14 mm for rotor B.

For non-Newtonian fluids, however, the calculated effective length of the gap can at best be interpreted as an approximative value. For this type of fluids the flow birefringence is often less than proportional to the shear rate q, whereas the extinction angle can considerably deviate from 45° (see e. g. fig. 9). In the case of Manolene 6050 Δn is roughly proportional to $q^{0.75}$ (fig. 8). This means that the contribution of the "main" velocity gradient q_{xy} near the windows, notwithstanding the fact that it drops down a little faster than in the Newtonian case, can even have more influence on Δn than in the Newtonian case. With the use of the above mentioned relation between birefringence and shear rate one can construct (in a similar way as has been done in fig. 7 for the velocity gradient q_{xy}) a curve of the local birefringence as a function of the dimensionless distance from one of the windows, e. g. for $q = 100\,s^{-1}$. It appears that the local birefringence curves for the Newtonian and the non-Newtonian cases coincide readily. This means that also in the case of Manolene 6050 the effective optical light path should be close to 7.14 mm.

So far, the role which the "parasitic" velocity gradient q_{xz} may play in the non-Newtonian case has not been discussed. According to fig. 7 the maximum value of q_{xz} is about 25% of the value of the nominal shear rate q_n. The surface under the curve of the dimensionless "parasitic" velocity gradient q_{xz} is about 7% of the surface under the dimensionless curve of the "main" velocity gradient q_{xy}. However, the situation is complicated by the fact that the extinction angle of the "main" birefringence deviates from 45° and at the same time, the parasitic birefringence increases with the rotational speed of the rotor. So far, no theoretical prediction about these influences has been made In this connection it should also be kept in mind that the fluid model of eq. [5] is not capable of predicting extinction positions.

In fact, as will be shown below, the experimental extinction angle curves, as obtained for different types of polymers, can be affected by the edge effect in a fundamentally different way.

5. Results and discussion

First we shall discuss some typical measurements which were obtained during steady shear flow. The following combinations were used:

Rotor A, 1° 8′ gap angle
Rotor A, 2° 17′ gap angle
Rotor B, 1° 8′ gap angle

The measurements at the lowest shear rates were obtained with the aid of an apparatus with coaxial cylinders. This apparatus was specially designed for the measurement of flow birefringence at extremely low shear rates and will be described elsewhere.

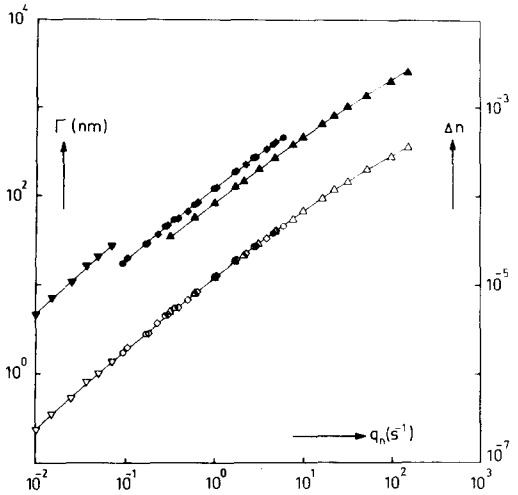

Fig. 8. Double logarithmic plot of the path difference Γ (filled symbols) and the flow birefringence Δn (open symbols) as functions of the nominal shear rate q_n, for high density polyethylene Manolene 6050 at a temperature of 179 °C:
(▽) ... coaxial cylinder apparatus,
(○) ... rotor A and 1° 8′ gap angle,
(◇) ... rotor A and 2° 17′ gap angle,
(△) ... rotor B and 1° 8′ gap angle

In fig. 8 the measured path difference $\Gamma = \frac{\delta \cdot \lambda}{2\pi}$ and the flow birefringence Δn are plotted as functions of nominal shear rate q_n for polyethylene Manolene 6050 at a temperature of 179 °C, where δ is the phase difference and λ is the wave length of the used light. In all cases $\lambda = 546.1$ nm. When the measured path differences are divided by the effective lengths of the respective light paths, the flow birefringences in the 1–2 plane (where 1 and 2 denote coordinates in the usual manner) are found. For rotor A the length of the effective light path is assumed to be 10 mm. If path differences, as obtained with the aid of rotor B, should produce birefringences Δn, that overlap with the ones obtained with rotor A, an effective light path of 7.0 mm has to be chosen. This experimentally found length agrees very well with the one calculated in the previous section. In this way it appears that the measured path difference, Γ, for Manolene 6050 is not seriously influenced by the parasitic velocity gradient. For rotor A and the different gap angles used, the measurements show that the path difference is independent of the gap angle.

The correctness of the path length of 10 mm, as assumed for rotor A, is also confirmed by the agreement of the birefringence values found with the coaxial cylinder apparatus.

Finally it can be emphasized that the new rotor B enables the measurement of the flow birefringence of Manolene 6050 over an additional decade in shear rate when compared with rotor A. This finding agrees with the conclusion drawn by *Wales* (21), i. e. that the depolarization of the light with rotor A at high shear rates, is due to the extra velocity gradients near the windows.

Fig. 9 shows the measured extinction angles χ as a function of nominal shear rate q_n for Manolene 6050 at a temperature of 179 °C. These extinction angles, which were obtained with rotor A and different gap angles, are independent of the chosen gap angle. In fig. 10 measurements are shown which were obtained on the same polyethylene using rotor B and gap angle 1° 8′ geometry. The measured extinction angles are plotted versus the nominal shear rate q_n. The dotted lines indicate the shear rates at which the phase difference, δ, becomes equal to $n.2\pi$ ($n = 1, 2, \ldots$). Near these "fringes" deviations can be noticed from the normal behaviour of the extinction angle curve. Just

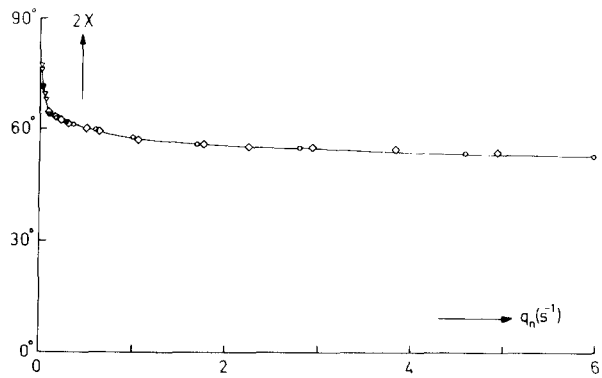

Fig. 9. Doubled extinction angles 2χ as a function of nominal shear rate q_n for high density polyethylene Manolene 6050 at a temperature of 179 °C:
(▽) ... coaxial cylinder apparatus,
(○) ... rotor A and 1° 8′ gap angle,
(◇) ... rotor A and 2° 17′ gap angle

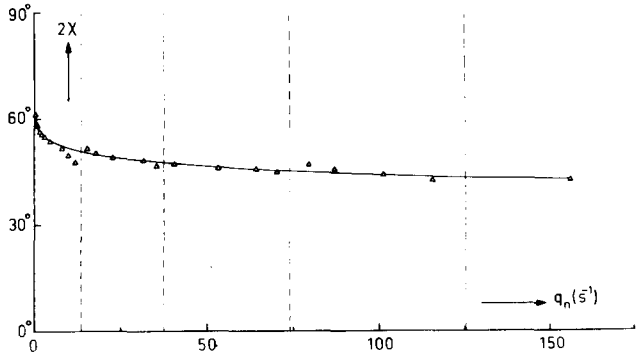

Fig. 10. Doubled extinction angle 2χ as a function of nominal shear rate q_n for high density polyethylene Manolene 6050 at a temperature of 179°C: (△)... rotor B and 1°8′ cone angle. The dotted lines indicate the shear rates where the phase difference is equal to $n \cdot 2\pi$ ($n = 1, 2, 3 \ldots$)

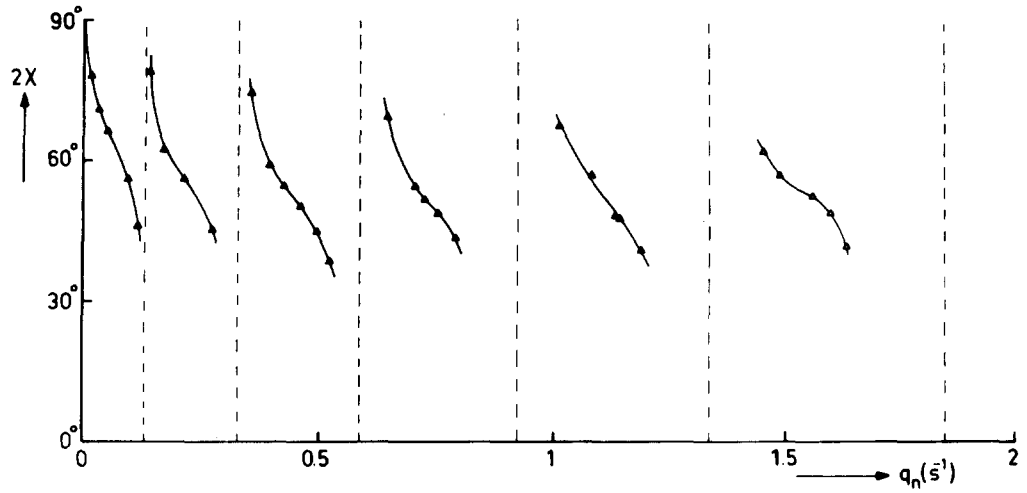

Fig. 11. Doubled extinction angle 2χ as a function of nominal shear rate q_n for polystyrene Hoechst at a temperature of 170°C: (△)... rotor B and 1°8′ gap angle.
The dotted lines indicate the shear rates where the phase difference is equal to $n \cdot 2\pi$ ($n = 1, 2, \ldots$)

before every "fringe" the extinction angle drops below the smoothed curve. Directly behind the fringe, an extinction angle is measured which seems somewhat too high.

A similar but more pronounced effect is observed for the polystyrene at 170°C, as shown in fig. 11. These results were obtained from data taken with the same combination of rotor B and cone as indicated previously for Manolene 6050 at 179°C. When figs. 10 and 11 are compared, one observes that many more fringes occur with polystyrene. This is due to the higher optical anisotropy of the polystyrene molecule. There is also a big difference in molecular weight (distribution). For the polystyrene sample the extinction angle curve is completely obscured in the higher shear rate range by the edge effect. This effect becomes predominant near the fringes where the path difference due to the main birefringence becomes virtually zero. It is shown in the appendix how the observed discontinuities in the experimental extinction angle can be understood. It is interesting to note that with the melt of a branched low density polyethylene, the *S*-shape parts of the extinction angle curve were found to have a positive slope in contrast to what is shown in figs. 10 and 11 for the linear polymers. This is shown in fig. 12. The measurements were obtained in the following way. The points of the first curve (open symbols) were obtained at increasing shear rates up to $6\,s^{-1}$. Before the points were taken, the steady state situation was always reached. The second curve (filled symbols) was obtained with decreasing shear rates. Within the indicated range of shear rates, the second curve is exactly reproducible. The big difference between these two curves is obviously a consequence of mechanical degradation. In fact viscous dissipation cannot

be made responsible for the phenomenon. One can learn from fig. 7 of *Meissner*'s report (23), that the viscosity of this polymer at $q = 6\,s^{-1}$ and a temperature of 150 °C is of the same order as the viscosity of Manolene 6050 at $q = 6\,s^{-1}$ and 179 °C. For the latter polymer no influence of viscous dissipation could be discovered.

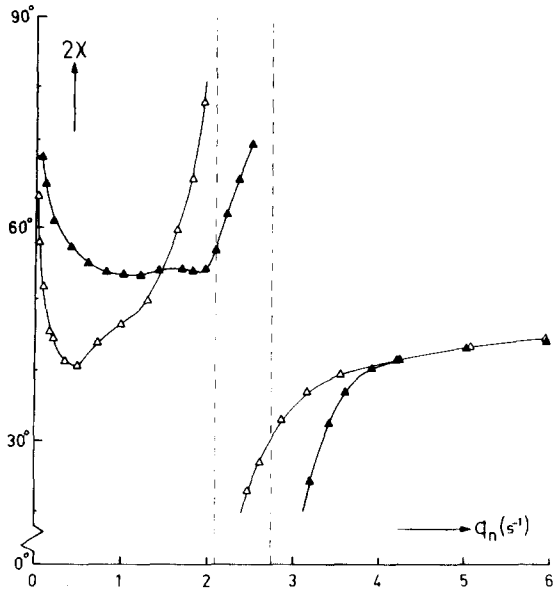

Fig. 12. Doubled extinction angle 2χ as a function of nominal shear rate q_n for low density polyethylene (IUPAC A) at a temperature of 150 °C: (△) ... rotor B and 1°8′ gap angle. Open symbols indicate increasing values of shear rate. Filled symbols indicate decreasing values of shear rate. The dotted lines show the shear rates where the phase difference is equal to 2π

The stress-optical law can be checked for Manolene 6050 in the whole range of applied shear rates using fig. 10. The stress-optical law can be expressed by the following relations (1):

$$\Delta n \sin 2\chi = 2C p_{12}, \qquad [6]$$

$$\Delta n \cos 2\chi = C(p_{11} - p_{22}), \qquad [7]$$

where p_{12} is the shear stress, $p_{11} - p_{22}$ the first normal stress difference, Δn the flow birefringence in the 1–2 plane and χ the extinction angle (as functions of q_n) and C the stress-optical coefficient. The validity of eq. [6] can be checked by plotting $\frac{\Delta n \sin 2\chi}{2p_{12}}$ as function of the nominal shear rate q_n. A constant value of this coefficient should be found. When eq. [7] is divided by eq. [6] one obtains:

$$\cot 2\chi = \frac{p_{11} - p_{22}}{2p_{12}}. \qquad [8]$$

This equation predicts the coaxility of the stress and refractive index tensors.

Fig. 13 shows the constancy of C for Manolene 6050 at a temperature of 179 °C over more than 4 decades in shear rate. Over the same range of shear rates, the viscosity (see fig. 4) decreased by a factor of 10. At shear rates of the order of $100\,s^{-1}$ the stress-optical coefficient starts to drop down. According to the calculations in section 3, however, this can be partly ascribed

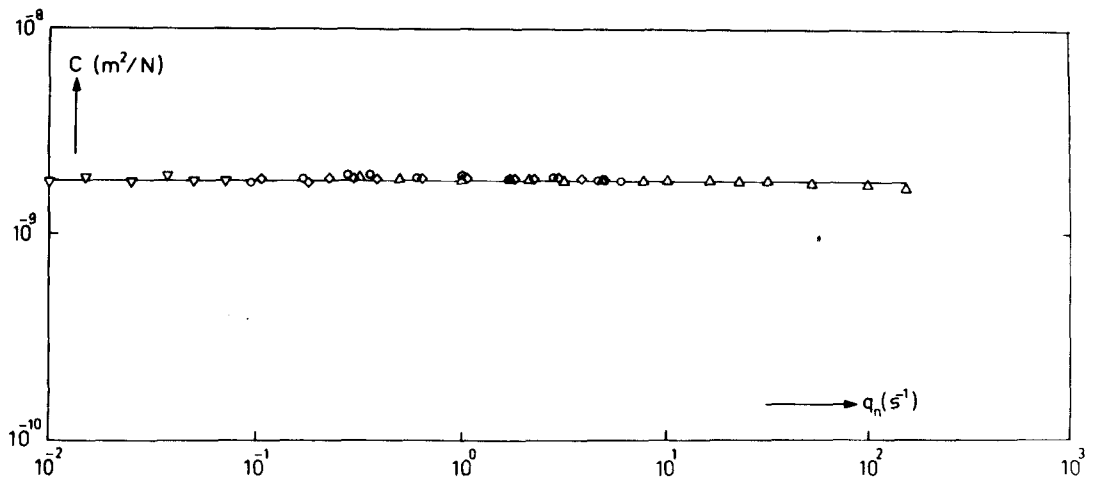

Fig. 13. Stress-optical coefficient C, as calculated from χ (figs. 9 and 10), Δn (fig. 8) and p_{12} (fig. 4), as a function of shear rate for high density polyethylene Manolene 6050 at a temperature of 179 °C:
(▽) ... coaxial cylinder apparatus, (○) ... rotor A and 1°8′ gap angle, (◇) ... rotor A and 2°17′ gap angle, (△) ... rotor B and 1°8′ gap angle

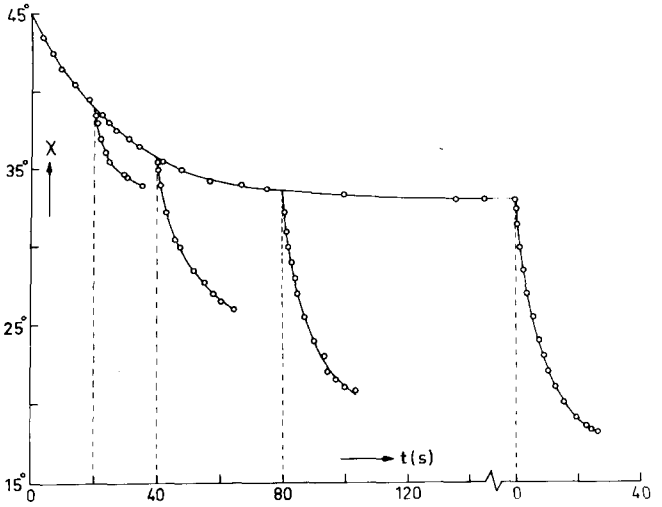

Fig. 14. Extinction angle χ as a function of time for polystyrene Hoechst at a shear rate $q_n = 0.05\,s^{-1}$ and a temperature of 170°C. At time zero flow was suddenly started. Flow was suddenly stopped after several total amounts of shear $\gamma_t (= q_n \cdot t$ equal to 1, 2 and 4) and after steady shear flow. Measurements were performed with rotor A and 1°8′ gap angle

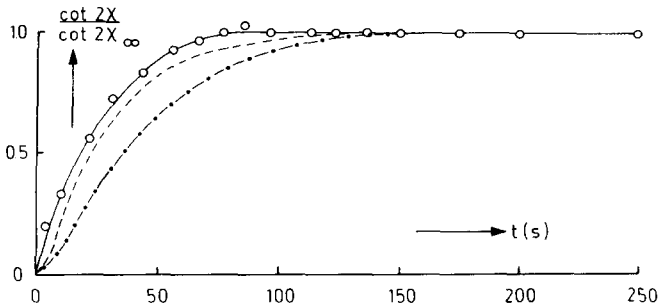

Fig. 15. Plots of the reduced stress ratios cot $2\chi_t$/cot $2\chi_\infty$ against time for polystyrene Hoechst at a temperature of 170°C and $q_n = 0.07\,s^{-1}$:
(○) ... optical measurements as obtained with rotor A and 1°8′ gap angle
(– – – –) ... mechanical measurements with 8° gap angle
(–·–·–) ... mechanical measurement with 4° gap angle

to viscous dissipation in the flow birefringence apparatus.

Finally, we shall discuss some typical transient measurements. The birefringence measurements were performed with rotor A and a gap angle of 1°8′. In fig. 14 results are shown of measurements of the transient extinction angle for the polystyrene sample at a shear rate $q_n = 0.05\,s^{-1}$ and a temperature of 170°C. At time zero the indicated shear rate was "suddenly" applied to the fluid at rest[2]). The corresponding extinction angle curve starts at 45° to the flow direction and levels off at its steady state value. Also relaxation of the extinction angle is shown. It occurs when flow is suddenly stopped after various total amounts of applied shear $\gamma_t (= q \cdot t$ equal to 1, 2, 4) and after steady shear flow. A consultation of eq. [8] shows that, in qualitative agreement with *Lodge*'s (26) prediction, the transient primary normal stress difference changes more slowly with time than the transient shear stress. This holds for the commencement as well as the cessation of flow. *Philippoff* and *Biss* obtained similar results on polyisobutene in white oil (31).

In order to corroborate this conclusion, evidence should be given of the validity of the assumed coaxiality of stress and refractive index tensors. For this purpose some direct transient measurements of $p_{11} - p_{22}$ must be carried out on a Weissenberg rheogoniometer. As already mentioned, Drs. *Laun* and *Münstedt* of BASF provided us with the needed results for our polystyrene sample. In fig. 15 a comparison is made between optical and mechanical measurements for a shear rate $q_n = 0.07\,s^{-1}$ at a temperature of 170°C. As recommended by *Meissner* (27), several gap angles were used for the mechanical measurements. According to *Meissner* a test like the one carried out with the 4 degree gap angle of the Weissenberg rheogoniometer can be expected to reflect a more retarded

[2]) "Suddenly" means that the time interval in which the shear rate is increased from zero to the nominal value (i.e. 10 ms) is small compared with the characteristic time scale of the polymer sample.

response of the apparatus than a test with the 8 degree gap angle. In fact, it appears from fig. 15 that the optically measured ratio, $\frac{p_{11}-p_{22}}{2p_{12}}$, increases more rapidly than the mechanically measured ratios, even if the gap angle is increased to 8 degrees. This could be expected because the flow birefringence measurements were performed with a very rigid apparatus. The three tests shown lead to nearly the same steady state value. At lower rates of shear, where the forces in the Weissenberg apparatus become smaller, almost complete agreement is found between optical and mechanical measurements. Details of this investigation will be given elsewhere. For the moment we can conclude that the coaxiality of stress and refractive index tensors is valid also for the transient situations considered. *Meissner*'s view on the influence of the gap angle on the measurement of time dependent normal stresses is substantiated by the optical measurements. Moreover, *Hansen* and *Nazem* (28) made a theoretical and experimental study to measure meaningful transient normal forces in the cone-and-plate geometry of the Weissenberg rheogoniometer, which is in full accordance with the present findings. Finally, it should be mentioned that the stress-optical coefficient of the investigated polystyrene has been found to be constant also in the transient region and that the mentioned coaxiality of the stress and refractive index tensors has previously been checked in steady shear flow for several polymers (21).

In the future high shear rate experiments will be carried out with a stationary plate and a rotating cone. In this way we hope to perform measurements near the stationary wall, where the parasitic velocity gradient q_{xz} becomes zero. With the present arrangement (see fig. 1) measurements near the stationary wall are impossible, since the light beam is intercepted at the inner rim of the stationary cone. The influence of the parasitic velocity gradients q_{xz} on the measurement of the extinction angle can probably be considerably reduced in this way. In this connection it is interesting to discuss the reasons for the fact that rotor B of the present paper allows sharp extinction readings in the high shear rate range where rotor A fails to give sharp extinction positions. We believe that the divergence of the light beam plays a role in this phenomenon. As a matter of fact, rotor B allows the adjustment of a dark line, which is directed parallel to the stream lines (i. e. the x-direction), in the center of the field. The pertinent reading on the vernier scale furnishes the "measured" extinction angle. If the parasitic velocity gradients near the window change more rapidly in the y-direction, this dark line becomes narrower and will therefore be visible only in a light beam consisting of strictly parallel rays. In a slightly unorderly beam, as resulting from unavoidable temperature gradients, etc., the narrow line will be dispersed by the divergence of the light rays.

Appendix: Influence of parasitic optical phase differences on the extinction angle

As no predictions can be made a priori about magnitude and extinction direction of the parasitic birefringences, we shall restrict ourselves to the derivation of a formula which relates the measured extinction angle to the "true" extinction angle and arbitrary but identical edge effects near both windows. This calculation can be carried out with the aid of a matrix method as developed by *Walker* (29) or with the aid of trigoniometric considerations on *Poincaré*'s sphere (30).

In our measuring device the light beam passes through the following optical components:

a) the polarizer making an angle χ ($< 45°$) with the direction of flow,
b) a parasitic birefringent medium showing an extinction angle χ_p (with regard to the direction of flow) and a phase difference δ_p,
c) the main birefringent medium showing an extinction angle χ_r (with respect to the direction of flow) and a phase difference δ_r,
d) another parasitic birefringent medium identical with the one mentioned under b) and
e) the analyser making an angle $\chi + \pi/2$ with the direction of flow.

In the case of extinction the mentioned calculation leads to the following expression:

$$\tan(2\chi - 2\chi_p) = \frac{\tan(2\chi_r - 2\chi_p)}{\cos\delta_p} \left[\frac{1}{1 + \frac{\tan\delta_p}{\cos(2\chi_r - 2\chi_p)\tan(\delta_r/2)}}\right]. \quad [9]$$

At this point it is interesting to note that, due to the large phase differences involved, no extinction will be possible for the case that the two parasitic effects differ from each other. As sharp extinctions are found in practice, at least the assumption of identical parasitic effects is justified.

In the same way the measured phase difference can be related to the "true" and parasitic effects. This formula, however, is not given. It shows that there should be no big differences between the measured and the "true" phase differences.

With the aid of eq. [9] the shape of the experimental extinction angle curves, as shown in figs, 10, 11 and 12, can roughly be generated if, for simplicity, certain constant values are assumed for χ_p, δ_p and χ_r for the shear rate range between two subsequent fringes, whereas the "true" phase difference δ_r is assumed to increase linearly with the shear rate. It depends on the sign of δ_p (with respect to that of δ_r) whether the type of linear polymers (reverse sign, figs. 10 and 11) or the branched polymer (equal sign, fig. 12) is produced. It can also be concluded that the deviation of χ from χ_r is positive near the inflection points.

Acknowledgements

The authors are grateful to *D. Eikelenboom, H. G. Langen* and *E. v. d. Velden* for their assistance in design, to *H. C. Nieuwpoort* and *G. de Vos* of the workshop of the Chemistry Department for the careful construction of the apparatus, to *M. J. Wijsman* of the Department of Physics for the construction of the high tolerance windows and mirror and to *R. van Donselaar* and *W. Verhoeff* for their advice with respect to the driving system and for the careful installation of the electrical equipment.

Thanks are also due to Dr. *J. L. S. Wales*, Central Laboratory T.N.O. for his very useful suggestions for the design of the apparatus and to Drs. *Laun* and *Münstedt* of BASF Ludwigshafen for providing the rheogoniometer data of the polystyrene and high density polyethylene samples investigated. The authors are also indebted to *K. te Nijenhuis* for discussions and for the permission to use his automatic dynamic viscometer. Thanks are also due to *W. C. M. Gorissen* and Prof. *J. F. Ingen Housz*, Twente University of Technology, for teaching the first author to solve flow problems similar to the one treated in section 4.

Summary

A description is given of a modified cone-and-plate apparatus designed for the measurement of the flow birefringence of polymer melts in a wide range of shear rates. Results are given of measurements on samples of high and low density polyethylene and polystyrene. Anomalies, as found in the extinction angle curves near the fringes, where the phase differences become equal to multiples of 2π, point to pronounced edge effects which appear to depend on the type of polymer. The measurements on the high density polyethylene were used to check the validity of the stress-optical law. The measurements on the low density polyethylene sample show mechanical degradation of this polymer. Some typical transient measurements on the polystyrene sample are presented and successfully related to the corresponding mechanical measurements, as obtained with the aid of a cone-and-plate Weissenberg rheogoniometer.

Zusammenfassung

Ein modifizierter Kegel-Platte-Apparat wird beschrieben, der entworfen wurde, um die Strömungsdoppelbrechung polymerer Schmelzen in einem großen Bereich von Schergeschwindigkeiten zu messen. Meßergebnisse an Proben von Polyäthylen hoher und niedriger Dichte, sowie von Polystyrol, werden wiedergegeben. Anomalien, die an den Auslöschungswinkelkurven in der Nähe der Ordnungen, bei denen der Phasenunterschied Vielfache von 2π beträgt, gefunden wurden, weisen auf ausgeprägte Randeffekte hin, die offenkundig von der Natur des Polymeren abhängen. Die Messungen an der Probe des Polyäthylens hoher Dichte wurden dazu verwendet, die Gültigkeit des spannungsoptischen Gesetzes zu prüfen. Die Messungen an der Probe des Polyäthylens niedriger Dichte zeigen mechanische Degradierung an. Einige typische Übergangsmessungen an der Polystyrolprobe werden beschrieben. Die erhaltenen Ergebnisse werden mit entsprechenden Ergebnissen mechanischer Messungen, die mit Hilfe des Weissenberg-Rheogoniometers erhalten wurden, verglichen, wobei die erwartete Übereinstimmung gefunden wurde.

References

1) *Janeschitz-Kriegl, H.*, Adv. Polymer Sci. **6**, 170 (1969).

2) *Garmonova, I. I.*, Vestn. Leningr. Univ., No. 22, 72 (1962).

3) *Brodnyan, J. G., F. H. Gaskins, W. Philippoff*, Trans. Soc. Rheol. **1**, 109 (1957).

4) *Philippoff, W.*, J. Polymer Sci. **57**, 141 (1962).

5) *Janeschitz-Kriegl, H., U. Daum*, Kolloid-Z. **210**, 112 (1966).

6) *Daum, U.*, J. Polymer Sci. A2, **6**, 141 (1968).

7) *Wayland, H.*, J. Polymer Sci., Part C, **5**, 11 (1964).

8) *Harris, J.*, Rheol. Acta **9**, 467 (1970).

9) *Janeschitz-Kriegl, H., F. H. Gortemaker*, Delft Prog. Rep. Series A **1**, 73 (1974).

10) *Wales, J. L. S.*, Rheol. Acta **8**, 38 (1968).

11) *Wales, J. L. S., W. Philippoff*, Rheol. Acta **12**, 25 (1973).

12) *Wales, J. L. S., H. Janeschitz-Kriegl*, J. Polymer Sci., A-2, **5**, 781 (1967).

13) *Shurcliff, W. A.*, Polarized Light; Production and Use (Cambridge, Mass. 1962).

14) *Ehringhaus, A.*, Z. Krist. **76**, 315 (1931).

15) *Bagley, E. B.*, J. Appl. Phys. **28**, 624 (1957).

16) see e. g. *Brydson, J. A.*, Flow Properties of Polymer Melts (London 1970).

17) *Den Otter, J. L.*, Doctoral Thesis, Leiden (1967), and Rheol. Acta **8**, 355 (1969).

18) *Morrison, T. E., L. J. Zapas, T. W. de Witt*, Rev. Sci. Instr. **26**, 357 (1955).

19) *Ferry, J. D.*, Viscoelastic Properties of Polymers, 2nd ed. (New York 1970).

20) *Cox, W. P., E. H. Merz*, J. Polymer Sci. **28**, 619 (1958).

21) *Wales, J. L. S.*, Doctoral Thesis, Delft (1976).

22) *Wales, J. L. S.*, Pure and Appl. Chem. **20**, 331 (1969).

23) *Meissner, J.*, Pure and Appl. Chem. **42**, 553 (1975).
24) *Hansen, M. G.*, Ph. D. dissertation, University of Wisconsin (Madison 1974).
25) *Gortemaker, F. H., B. de Cindio, H. Janeschitz-Kriegl*, in preparation.
26) *Lodge, A. S.*, Elastic Liquids (London-New York 1964).
27) *Meissner, J.*, J. Appl. Polym. Sci. **16**, 2877 (1972).
28) *Hansen, M. G., F. Nazem*, Trans. Soc. Rheol. **19**, 21 (1975).
29) *Walker, M. J.*, Am. J. Phys. **22**, 170 (1954).
30) *Poincaré, H.*, Traité de la Lumière (Paris 1892).
31) *Philippoff, W., R. Biss*, personal communication.

Authors' addresses:

Prof. Dr. *H. Janeschitz-Kriegl*
Dr. *F. H. Gortemaker*
Laboratory of Physical Chemistry
Delft Technical University
Julianalaan 136
Delft 8 (The Netherlands)

Dr. *M. G. Hansen*
General Electric Research Laboratories
Schenectady, N. Y. (USA)

Dr. *B. de Cindio*
Istituto di Principi di Ingegneria Chimica
University of Naples (Italy)